Calibration and Evaluation of Precipitable Water Vapor From MODIS Infrared Observations at Night

Liang Chang, *Member, IEEE*, Guoping Gao, Shuanggen Jin, Xiufeng He, Ruya Xiao, and Lixin Guo

***Abstract*—Water vapor is one of the most variable atmospheric constituents. Knowledge of both the spatial and temporal variations of atmospheric water vapor is very important in forecasting regional weather and understanding the global climate system. The Moderate Resolution Imaging Spectroradiometer (MODIS) is the first space instrument to obtain precipitable water vapor (PWV) with near-infrared (nIR) bands and the traditional IR bands, which provides an opportunity to monitor PWV with wide coverage during both daytime and nighttime. However, the accuracy of PWV measurements obtained with IR bands is much lower than that with nIR bands. Moreover, seldom have studies been devoted to the calibrations of MODIS IR PWV. In this paper, the accuracy of MODIS IR water vapor product during the nighttime is assessed by ERA-Interim data, Global Positioning System, and radiosonde observations. Results reveal that the performance of MODIS IR water vapor product is much poorer than that from the other observations, and the MODIS IR PWV needs to be calibrated. As such, we propose a differential linear calibration model (DLCM) to calibrate the MODIS IR water vapor product during the nighttime. Case studies under both dry and moist atmosphere in midlatitude and equatorial regions are used to test and assess the performance of the DLCM. Results show that the DLCM can effectively enhance the accuracy of MODIS IR retrievals at nighttime. Furthermore, while the traditional least square model may over calibrate the MODIS IR PWV measurements occasionally, the DLCM can avoid that defect successfully.**

***Index Terms*—Calibration model, infrared (IR), Moderate Resolution Imaging Spectroradiometer (MODIS), night, water vapor.**

I. Introduction

ATMOSPHERIC water vapor is the most important greenhouse gas and plays a crucial role in understanding and predicting the Earth's climate change. The phase variability of water vapor in time and space over a large range scale affects the vertical stability of the atmosphere, the evolution of the weather, and the energy balance of the global climate system [1]. Precipitable water vapor (PWV), which is also referred to as total column or integrated water vapor, is the total water vapor contained in an air column from the Earth's surface to the top of the atmosphere, and it is a good indicator of the variability of water vapor in the lower troposphere and related processes [2].

The traditional radiosonde technique has long been the primary *in situ* observing system for detecting global atmospheric water vapor, and it also represents an increasingly valuable resource for studies of climate change [3]. However, global radiosonde observations are only available twice a day, and they often contain systematic biases [4] and spurious changes [5]. In addition, the use of radiosonde is limited due to their high operational costs and their poor coverage over oceans and in the southern hemisphere [6].

Global Positioning System (GPS) is another practical tool for measuring PWV on a global basis, which uses the delay in radio signals due to the permanent dipole moment of atmospheric water vapor molecules to infer PWV [7]. The advantages of the GPS-derived PWV involve continuous measurements in all weather conditions, high accuracy (at the level of 1–2 mm), long-term stability, and low cost [8]. Unfortunately, similar with radiosonde observations, GPS data are available usually only over land.

Spaceborne monitoring is strictly the only effective technique to evaluate water vapor distribution on a global scale. Currently, a number of sensors onboard satellite platforms have been implemented to observe water vapor amount, such as the Moderate Resolution Imaging Spectroradiometer (MODIS) [9] on Terra and Aqua platforms, the Medium Resolution Imaging Spectrometer (MERIS) [10] on Environmental Satellite platform, the Atmospheric Infrared Sounder (AIRS) [11] onboard Aqua, the Infrared Atmospheric Sounding Interferometer [12] onboard MetOp, the Microwave Radiometers (MWR) [13] onboard TOPEX/Poseidon and Jason, the Tropical Rainfall Measuring Mission's Microwave Imager (TMI) [14], and the recently launched Global Precipitation Measurement Microwave Imager [14]. The space-based instruments that detect infrared (IR) or (and) near-infrared (nIR) frequencies can measure moisture over both land and ocean regions, but only information collected under cloud-free conditions can be used, as the IR and nIR measurements are sensitive to the presence of clouds in the field of view. Furthermore, the IR retrievals (e.g., AIRS

Manuscript received September 28, 2013; revised February 16, 2014, June 20, 2014, August 3, 2014, and September 14, 2014; accepted September 25, 2014. This work was supported in part by the National Natural Science Foundation of China under Grant 41276197, by the Shanghai Pujiang Program under Grant 12PJ1404100, by the Shanghai Sailing Program under Grant 14YF1410200, by the Innovation Program of Shanghai Municipal Education Commission under Grant 14YZ118 and Grant 14ZZ148, by the Young Teacher Training Program of Shanghai Colleges and Universities under Grant A1-2035-14-0010-12, and by the Science Foundation for Doctors of Shanghai Ocean University under Grant A-0209-13-0105395. *(Corresponding author: Guoping Gao.)*

L. Chang, G. Gao, and L. Guo are with the College of Marine Sciences, Shanghai Ocean University, Shanghai 201306, China, and also with the Collaborative Innovation Center for Distant-water Fisheries, Shanghai 201306, China (e-mail: chlbwinds@hotmail.com; gpgao@shou.edu.cn; guolixin@163.com).

S. Jin is with the Shanghai Astronomical Observatory, Chinese Academy of Sciences, Shanghai 200030, China (e-mail: sgjin@shao.ac.cn).

X. He and R. Xiao are with the School of Earth Sciences and Engineering, Hohai University, Nanjing 210098, China (e-mail: xfhe@hhu.edu.cn; ruya.xiao@gmail.com).

Color versions of one or more of the figures in this paper are available online at http://ieeexplore.ieee.org.

Digital Object Identifier 10.1109/TGRS.2014.2363089

0196-2892 © 2014 IEEE. Personal use is permitted, but republication/redistribution requires IEEE permission.
See http://www.ieee.org/publications_standards/publications/rights/index.html for more information.

and MODIS) can be obtained during both the daytime and the nighttime, whereas the nIR retrievals (e.g., MERIS) are available in the daytime only. In this paper, we focus on the need for monitoring water vapor during the night, when water vapor transportation from the atmosphere to the ground surface makes important contributions to the water budget, particularly in arid and semiarid regions.

MODIS is the first space instrument that uses both nIR and IR bands to obtain global PWV distribution. However, comparing with the nIR water vapor retrievals, the accuracy of IR retrievals was much poorer. Thus, most of the studies were focused on the calibration and applications of nIR water vapor measurements (e.g., [6], [15], and [16]), whereas only a few studies have contributed to the analyses of IR retrievals at night (e.g., [17]–[19]), and seldom have works been devoted to the calibration of MODIS PWV at IR band during the nighttime. In this paper, we present a differential linear calibration model (DLCM) to calibrate the MODIS IR water vapor product at night. The accuracy of the calibration will be assessed with ERA-Interim data and GPS observations.

This paper is organized as follows. In Section II, the accuracy of MODIS IR water vapor product was analyzed via comparisons with PWV measurements from ERA-Interim data, GPS, and radiosonde observations. Calibrations of MODIS IR water vapor data with the proposed DLCM were discussed in Section III. Case studies of MODIS IR water vapor product calibrations and their assessments are presented in Section IV at middle- and low-altitude regions. Finally, some conclusions are addressed in Section V.

II. Accuracy Analysis of MODIS IR PWV Product

A. MODIS IR Water Vapor Data

The operational MODIS IR algorithm, which is implemented by a statistical regression algorithm together with an option of a subsequent nonlinear physical retrieval, is used for retrieving vertical temperature and moisture profiles, ozone profiles, PWV, and several atmospheric stability indices [17]. The MODIS IR water vapor retrievals are derived from band 24 to band 36 (between 4.47 and 14.24 μm), excluding band 26, and performed using clear-sky radiances measured within a 5×5 field of view (approximately 5-km resolution) over land and ocean for both day and night. The PWV measurements from the IR bands are generated as one component of the product MOD07 and simply added to product MOD05 for convenience.

In this paper, the MODIS level-2 water vapor and cloud mask product at IR band are obtained from the National Aeronautics and Space Administration (NASA) Goddard Earth Sciences Distributed Active Archive Center (http://daac.gsfc.nasa.gov). Moreover, it is noteworthy that the MODIS IR retrievals need to be calibrated before their applications due to the lower accuracy of the IR retrievals, which is one of the most prominent disadvantages for the MODIS IR water vapor product.

B. Other Data Used for Comparisons and Analyses

GPS is a powerful instrument for PWV monitoring with high temporal resolution and high precision, which could be regarded as a reference data set to assess MODIS PWV. In order to estimate PWV from GPS data, surface meteorological observations (i.e., pressure and temperature) collected at the GPS sites are required. However, the meteorological data were unavailable usually, even for the International GNSS Service network. In this paper, the GPS observations with surface meteorological sensors from SuomiNet [8] are being incorporated for comparisons and analyses. The PWV product from SuomiNet at 30-min sampling can be accessed at http://www.suominet.ucar.edu/data/index.html.

Quality-checked radiosonde data were retrieved from The British Atmospheric Data Centre (BADC, http://badc.nerc.ac.uk). For the purpose of the comparison of radiosonde estimates of PWV with MODIS IR water vapor product, the PWV measurements in millimeters from radiosonde observations were calculated in the following way:

$$\mathrm{PWV} = \frac{\left(\int_{z_0}^{z_1} \rho_v(z)\, dz\right)}{\rho_0} \tag{1}$$

where ρ_0 is the density of the water in kilograms per cubic meter, and $\rho_v(z)$ is the water vapor density in grams per cubic meter measured by the radiosonde as a function of altitude in meters between the surface altitude z_0 and the highest altitude z_1 where humidity data are recorded by the radiosonde.

ERA-Interim [20] is a third-generation and the latest global atmospheric reanalysis, which uses a much improved atmospheric model and assimilation system from those used in ERA-40. ERA-Interim represents a major undertaking by the European Centre for Medium-Range Weather Forecasts (ECMWF) with several of the inaccuracies exhibited by ERA-40 being eliminated or significantly reduced. In this paper, total column water vapor from ERA-Interim reanalysis at full resolution (i.e., $0.75^\circ \times 0.75^\circ$ grids) every 6 h (i.e., 00h, 06h, 12h, and 18h UTC) was adopted for the comparison and analyses of MODIS IR water vapor data. The data were retrieved from http://apps.ecmwf.int/datasets/data/interim_full_daily/.

C. Data Comparisons

The MODIS level-2 IR water vapor data (MOD05 products) collected from the Aqua satellite between May 1 and May 31, 2011, during the nighttime over the center of the United States (longitude: 110° W-100° W; latitude: 35° N-45° N; see Fig. 1) are compared with PWV measurements estimated from GPS, radiosonde, and ERA-Interim data. As MODIS PWV is sensitive to the presence of clouds, only IR retrievals that are 99% confidence clear are extracted for further analyses. In order to obtain PWV values from GPS, radiosonde, and ERA-Interim data at MODIS acquisition time, interpolation in time domain is performed using cubic splines. In addition, MODIS pixels were identified with the closest geographical coordinates to each GPS, radiosonde, and ERA-Interim location. In mountainous areas in Fig. 1, large differences and biases are detected during the comparisons among PWV measurements from GPS, radiosonde, and ERA-Interim data. In order to make the comparisons more objective, we perform the analysis with small and large altitude differences separately (see Fig. 2).

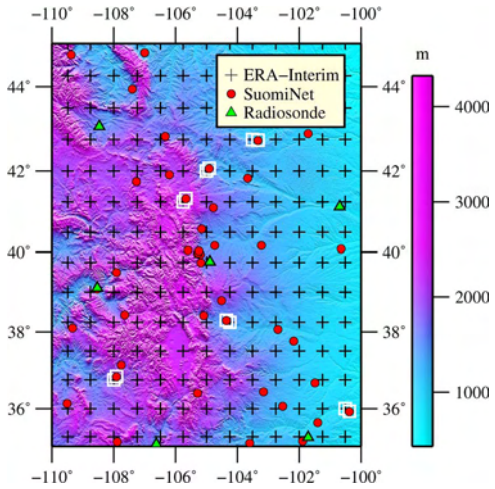

Fig. 1. Distributions of radiosonde observations, SuomiNet sites, and ERA-Interim grids superimposed on GTOPO30 (http://edc.usgs.gov/products/elevation/gtopo30/gtopo30.html). Black pluses represent ERA-Interim grids, red solid squares are GPS stations of SuomiNet, and green triangles denote radiosonde observations. The white empty squares show the pairs of ERA-Interim grids and SuomiNet sites within a given distance (e.g., 15 km in this study).

It can be inferred from the comparisons in Fig. 2(a)–(e) that the MODIS IR values appeared to be overestimated for a dry atmosphere and underestimated for a wet atmosphere, which is consistent with the analyses of previous studies [17], [18]. Furthermore, the performance of IR retrievals when compared with radiosonde observations [see Fig. 2(a)] is much poorer [i.e., the root mean square (RMS) was larger than 3 mm, and the standard deviation (STD) of the mean difference was close to 3 mm] than that with GPS and ERA-Interim reanalysis, which is mainly due to the radiosonde drift. Fig. 2(b) and (c) shows the comparisons between MODIS IR and GPS PWV, with their altitude difference below and above 100 m, respectively. The RMS difference and the STD between MODIS IR and GPS PWV are 2.22 and 0.84 mm [see Fig. 2(c)], respectively. The deviations of MODIS IR PWV from GPS PWV in Fig. 2(c) could lie in the fact that MODIS is averaging different altitudes within the scene, whereas GPS is referring to a specific point. However, when the altitude difference is small [i.e., less than 100 m in Fig. 2(b)], the large uncertainties of MODIS IR PWV measurements still exist, and no obvious improvements are observed (i.e., an RMS of 2.49 mm and an STD of 2.0 mm). The comparisons between MODIS IR and ERA-Interim PWV in both small and large altitude difference cases [see Fig. 2(d) and (e)] also show similar results to Fig. 2(b) and (c). The RMS differences of PWV measurements collocated in time and space are 2.58 and 1.96 mm, and the STDs are 2.34 and 1.58 mm in Fig. 2(d) and (e), respectively. The probable cause for the difference in Fig. 2(e) may be the poor performance of the numerical models in mountainous regions, as well as the approximation in the surface altitude, from which the derived PWV measurements are highly dependent. Moreover, the main reason for the poor performance in Fig. 2(d) with small altitude difference may be due to the altitude difference between MODIS and ERA-Interim PWV measurements, together with the low accuracy of the MODIS IR retrievals. Therefore, the MODIS IR water vapor should be properly calibrated for water vapor monitoring.

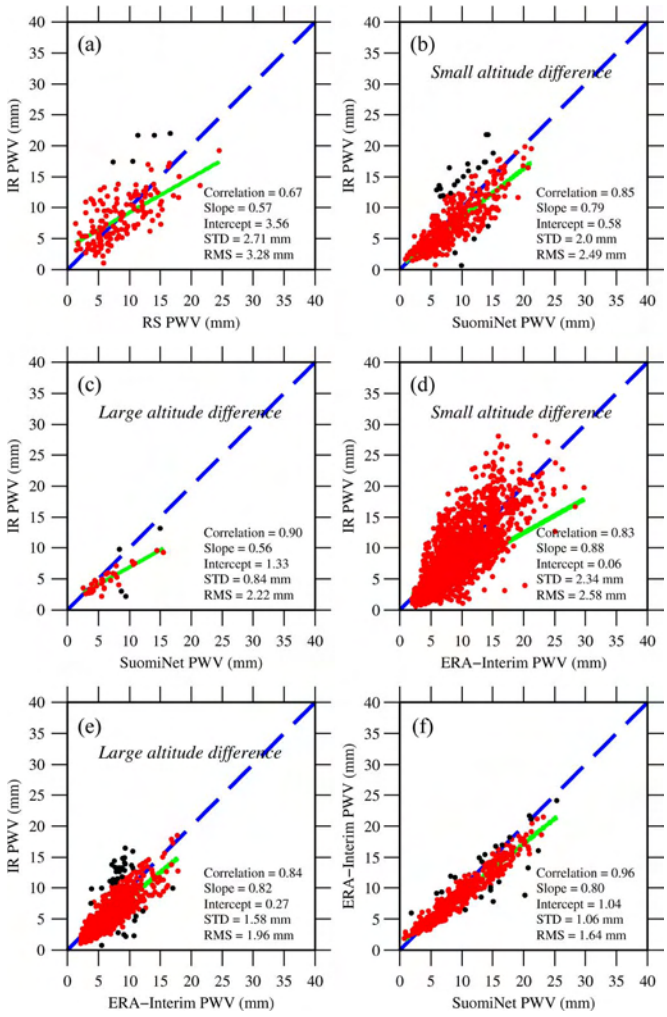

Fig. 2. Spatiotemporal comparisons among PWV measurements from MODIS IR water vapor product, radiosonde observations, SuomiNet observations, and ERA-Interim data. (a) MODIS IR PWV and radiosonde PWV. (b) MODIS IR PWV and SuomiNet PWV with small altitude difference. (c) Similar to (b), but with large altitude difference. (d) MODIS IR PWV and ERA-Interim PWV with small altitude difference. (e) Similar to (d), but with small altitude difference. (f) ERA-Interim PWV and SuomiNet PWV. Note that the black solid circles are considered as outliers and are removed due to the 2σ exclusion. The linear regression is shown as the green line, and the blue dash line is the zero bias.

III. DLCM

A. Model Construction and Implementation

Although the MODIS IR water vapor product can be available at both daytime and nighttime, the advantage in temporal scale has not attracted more attention due to its poorer accuracy. In order to take full advantage of the MODIS IR retrievals, we develop a DLCM for the MODIS IR water vapor product. The DLCM can be performed as follows (see Fig. 3).

1) Obtain the PWV measurements within the coverage area of MODIS image from reliable tools (e.g., GPS, radiosonde, ECMWF, or MWR) and estimate the reference PWV values for calibration at the MODIS overpass time (designated hereafter as $\mathrm{PWV}_{\mathrm{REF\_CAL}}$) by temporal interpolation (e.g., spline interpolation).
2) Extract the original PWV values from the MODIS IR water vapor product (designated hereafter as $\mathrm{PWV}_{\mathrm{ORIG}}$)

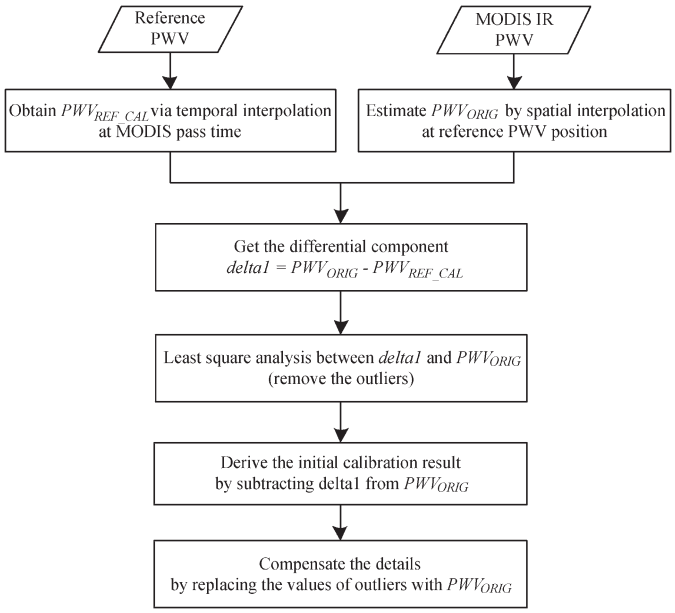

Fig. 3. Flowchart of the DLCM.

at the location of $\mathrm{PWV}_{\mathrm{REF\_CAL}}$ in (1) by spatial interpolation (e.g., inverse distance weight interpolation).

3) Subtract $\mathrm{PWV}_{\mathrm{REF\_CAL}}$ from $\mathrm{PWV}_{\mathrm{ORIG}}$ to get their differential component, which is defined as $\mathrm{delta1} = \mathrm{PWV}_{\mathrm{ORIG}} - \mathrm{PWV}_{\mathrm{REF\_CAL}}$, and then, implement the traditional linear least square (designated hereafter as LS) analysis between delta1 and $\mathrm{PWV}_{\mathrm{ORIG}}$ to derive the calibration coefficients and calibrate delta1. Note that those data points with a difference between delta1 and $\mathrm{PWV}_{\mathrm{ORIG}}$ exceeding twice the STD should be removed.
4) Subtract again the calibrated delta1 from $\mathrm{PWV}_{\mathrm{ORIG}}$, and the derived difference is recognized as the initial calibration of $\mathrm{PWV}_{\mathrm{ORIG}}$.
5) Considering that some reference values from $\mathrm{PWV}_{\mathrm{REF\_CAL}}$ with pretty large differences from $\mathrm{PWV}_{\mathrm{ORIG}}$ may be recognized as outliers and be omitted during the calibration, we compensate the moisture information of MODIS IR retrievals by replacing the corresponding values of $\mathrm{PWV}_{\mathrm{ORIG}}$ with that from $\mathrm{PWV}_{\mathrm{REF\_CAL}}$ and get the final calibrated $\mathrm{PWV}_{\mathrm{ORIG}}$ from the DLCM (designated $\mathrm{PWV}_{\mathrm{DLCM}}$ hereafter).

From the steps of the DLCM described above, we can see that the LS model is also adopted in the DLCM. The main difference of the DLCM from the LS model lies in that the former performs the regression analysis between $\mathrm{PWV}_{\mathrm{ORIG}}$ and its differential component from $\mathrm{PWV}_{\mathrm{REF\_CAL}}$, whereas the latter do that between $\mathrm{PWV}_{\mathrm{ORIG}}$ and $\mathrm{PWV}_{\mathrm{REF\_CAL}}$ directly. In addition, comparing with the outliers being removed directly when in the LS model, the proposed DLCM includes a refinement (i.e., step 5) during the calibration.

For MODIS nIR water vapor product calibration, the LS model has been proven to be a robust and effective calibration method [6], [19]. In this paper, the LS model will be also adopted to calibrate the MODIS IR water vapor product. Moreover, calibrations of MODIS IR water vapor with the LS model and the DLCM during the night period at middle and low altitudes will be analyzed in the next section.

TABLE I
BASIC PARAMETERS OF MODIS IR WATER VAPOR PRODUCT USED DURING THE NIGHTTIME

MODIS Scene	Date	Latitude	Min. PWV (mm)	Max. PWV (mm)	Mean PWV (mm)
MOD1	2011 Dec. 4	28.3° N ~ 49.6° N	0.58	29.43	6.98
MOD2	2009 Jul. 19	27.0° N ~ 48.3° N	1.54	71.37	38.07
MOD3	2009 Jan. 22	12.6° N ~ 33.6° N	3.58	49.22	18.03
MOD4	2011 May 13	13.7° N ~ 34.7° N	17.91	61.65	43.45

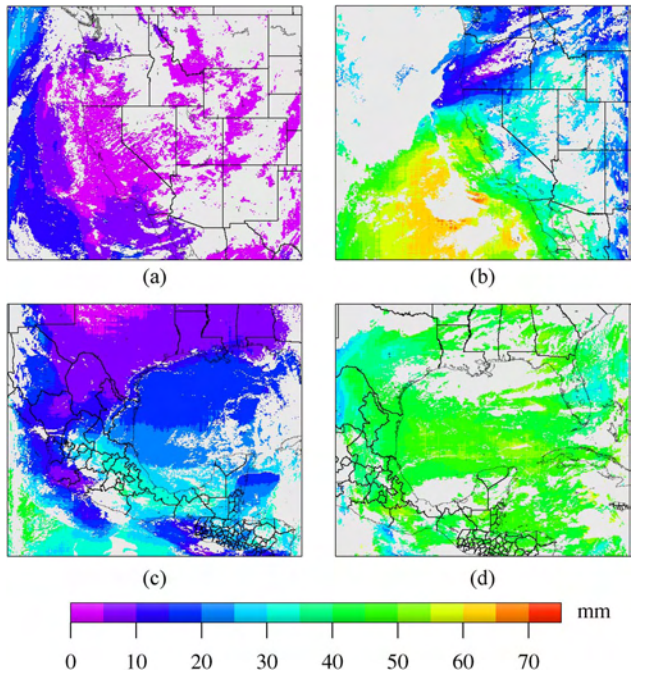

Fig. 4. PWV distributions retrieved from MODIS IR water vapor product at nighttime. (a)–(d) MODIS IR PWV fields collected on December 4, 2011; July 19, 2009; January 22, 2009; and May 13, 2011, respectively. (a) MOD1. (b) MOD2. (c) MOD3. (d) MOD4.

B. Reference PWV Measurements for Calibration

In order to calibrate the MODIS IR water vapor product with the DLCM effectively, accurate $\mathrm{PWV}_{\mathrm{REF\_CAL}}$ are required. Although the radiosonde can detect PWV with high accuracy, the derived PWV measurements are not the best choices to be selected as $\mathrm{PWV}_{\mathrm{REF\_CAL}}$ due to its sparse temporal and spatial distribution. GPS is an effective tool that can derive the PWV measurements with good accuracy and dense distribution, and it is therefore incorporated to produce the $\mathrm{PWV}_{\mathrm{REF\_CAL}}$ in this study. In addition, ERA-Interim reanalysis provides the global total column water vapor at 0.75° spatial resolution, which could be also another potential data set for $\mathrm{PWV}_{\mathrm{REF\_CAL}}$.

Fig. 2(f) shows the comparisons of PWV measurements from ERA-Interim reanalysis data and SuomiNet GPS observations (designated hereafter as $\mathrm{PWV}_{\mathrm{GPS}}$ and $\mathrm{PWV}_{\mathrm{ERA}}$, respectively). It should be noted that only data pairs between ERA-Interim grids and SuomiNet sites within a distance of 15 km were extracted for comparisons. It can be observed from Fig. 2(f) that $\mathrm{PWV}_{\mathrm{ERA}}$ matches $\mathrm{PWV}_{\mathrm{GPS}}$ quite well with high correlation. The RMS difference is 1.64 mm, and the STD of mean difference is about 1 mm. This consistency makes the ERA-Interim reanalysis an ideal reference data set to calibrate the

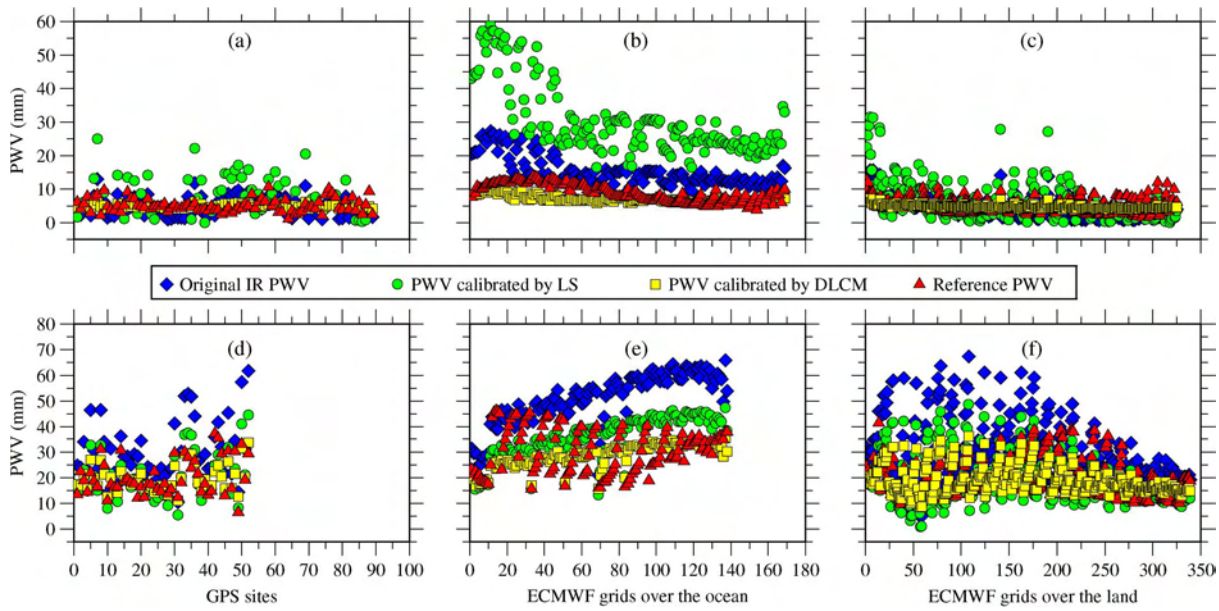

Fig. 5. Calibrations of MODIS IR PWV measurements in midlatitude regions when PWV_{GPS} is used as PWV_{REF_CAL}. The original and calibrated MOD1 PWV measurements were compared with (a) PWV_{GPS} and PWV_{ERA} over both (b) ocean and (c) land, respectively. (d)–(f) Similar to (a)–(c), but for water vapor field under wet atmosphere (i.e., MOD2).

performance of the DLCM. Moreover, in order to exclude the errors of PWV_{ERA} in mountainous areas, when PWV_{ERA} is used as PWV_{REF_CAL}, we remove the data points with the difference between PWV_{ERA} and PWV_{ORIG} exceeding twice the STD. Thus, both PWV_{GPS} and PWV_{ERA} are used as PWV_{REF_CAL} in this paper, respectively.

IV. Calibration of MODIS IR Water Vapor in Different Latitude Regions

A. Study Area and MODIS IR Water Vapor Data

Four MODIS IR water vapor scenes acquired in midlatitude (i.e., MOD1 and MOD2) and equatorial (i.e., MOD3 and MOD4) regions are used for the DLCM calibration analyses (see Table I). Both dry and moist cases in these regions are adopted to test the performance of the proposed calibration model (i.e., DLCM).

As the MODIS water vapor product is sensitive to the presence of clouds, and the frequency of global cloud coverage is pretty high (e.g., as high as 88% for July 28, 2008 [21]), invalid values are often found in MODIS-derived water vapor field. In this paper, only MODIS pixels collected under clear-sky conditions are retained for further analysis (see Fig. 4). The basic parameters of the IR scenes are listed in Table I.

B. Case Studies at Middle Latitude

Two calibrated MODIS IR water vapor fields via traditional LS method, as well as the proposed DLCM under dry (i.e., MOD1) and wet (i.e., MOD2) atmosphere in midlatitude regions, are compared and analyzed here, respectively. In order to evaluate the performance of the DLCM objectively, reliable reference PWV measurements for comparison (designated hereafter as PWV_{REF_COM}) are also needed. In this paper, both PWV_{GPS} and PWV_{ERA} are selected as PWV_{REF_COM}. As a result, both the internal and external coincidence precision can be estimated via difference choices of PWV_{REF_CAL} and PWV_{REF_COM}. The former can be achieved by selecting the same data set for PWV_{REF_CAL} and PWV_{REF_COM}, whereas the latter is evaluated by calibrating the MODIS IR PWV and comparing the calibrations with different data sets. Accuracy analyses of PWV_{ORIG}, PWV measurements calibrated by the LS model (designated as PWV_{LS} hereafter), and PWV_{DLCM} for MOD1 and MOD2 are shown in Fig. 5.

Selecting PWV_{GPS} as PWV_{REF_CAL}, the internal coincidence comparisons of PWV_{ORIG} and calibrated MOD1 IR retrievals with PWV_{GPS} are shown in Fig. 5(a), whereas the external coincidence comparisons of PWV_{ORIG} and calibrated MOD1 IR retrievals with PWV_{ERA} over both ocean and land are shown in Fig. 5(b) and (c), respectively. It is clear in Fig. 5(a) that large deviations exist between PWV_{ORIG} and PWV_{GPS}. The STD of the mean difference and the RMS difference are 2.65 and 2.81 mm (see Table II), respectively, during the comparison between PWV_{ORIG} and PWV_{GPS} in Fig. 5(a). After calibrating via the LS model, the STD and the RMS between PWV_{LS} and PWV_{GPS}, however, increase to 6.33 and 6.29 mm, respectively. In addition, when comparing PWV_{LS} with PWV_{ERA} over both land and ocean, the PWV_{LS} in Fig. 5(b) and (c) is also overcalibrated. The probable cause for this overcalibration may have resulted from the low correlation coefficient between PWV_{ORIG} and PWV_{GPS} (i.e., 0.36). In other words, the relationship between PWV_{ORIG} and PWV_{GPS} is not linear in Fig. 5(a)–(c). Fortunately, during the implementation of the proposed DLCM, the correlation coefficient between PWV_{ORIG} and delta1 ascends to 0.75, which results in a better agreement of PWV_{DLCM} with PWV_{REF_COM}. Taking the external coincidence comparisons as example, the STD of the mean difference between PWV_{DLCM} and PWV_{ERA} over land decreases from 3.52 to 0.76 mm, together with the RMS difference reduction from 7.18 to 2.79 mm (see Table II).

TABLE II
STD OF THE MEAN DIFFERENCES AND RMS DIFFERENCES OF PWV_{ORIG}, PWV_{LS}, AND PWV_{DLCM} AGAINST PWV_{REF_COM} FOR MOD1, MOD2, MOD3, AND MOD4, RESPECTIVELY (UNIT: MILLIMETERS)

MODIS Image	PWV_{REF_CAL}	PWV_{REF_COM}	PWV_{ORIG}		PWV_{LS}		PWV_{DLCM}		Corr. Figure
			STD	RMS	STD	RMS	STD	RMS	
MOD1	GPS	GPS	2.65	2.81	6.33	6.29	0.57	1.86	Fig. 5(a)
		ECMWF (Land)	3.52	7.18	8.41	23.32	0.76	2.79	Fig. 5(c)
		ECMWF (Ocean)	2.18	2.42	5.20	5.74	0.47	1.77	Fig. 5(b)
	ECMWF	GPS	2.65	2.81	1.59	2.12	0.92	1.87	Fig. 6(a)
		ECMWF	3.90	4.63	2.34	2.34	1.34	1.76	Fig. 6(b)
MOD2	GPS	GPS	7.48	12.52	5.69	5.58	3.29	4.48	Fig. 5(d)
		ECMWF (Land)	10.35	23.05	7.87	11.43	4.56	8.98	Fig. 5(f)
		ECMWF (Ocean)	7.75	12.18	5.89	5.90	3.41	4.75	Fig. 5(e)
	ECMWF	GPS	7.48	12.52	6.09	6.01	3.18	4.50	Fig. 6(c)
		ECMWF	10.23	16.10	8.33	8.36	4.35	6.30	Fig. 6(d)
MOD3	GPS	GPS	2.18	5.19	1.44	1.41	1.41	1.38	Fig. 7(a)
		ECMWF (Land)	2.88	9.34	1.91	5.14	1.87	5.19	Fig. 7(c)
		ECMWF (Ocean)	3.77	4.85	2.50	4.09	2.45	4.16	Fig. 7(b)
	ECMWF	GPS	2.18	5.19	2.22	3.94	1.67	1.91	Fig. 8(a)
		ECMWF	4.57	6.69	4.65	4.64	3.51	4.14	Fig. 8(b)
MOD4	GPS	GPS	2.95	5.89	2.41	1.96	1.93	1.76	Fig. 7(d)
		ECMWF (Land)	3.69	3.75	3.01	5.77	2.41	5.53	Fig. 7(f)
		ECMWF (Ocean)	4.86	5.02	3.96	6.09	3.18	5.55	Fig. 7(e)
	ECMWF	GPS	2.95	5.89	3.67	6.54	1.71	4.57	Fig. 8(c)
		ECMWF	4.29	4.41	5.34	5.33	2.48	3.71	Fig. 8(d)

When PWV_{GPS} is used as PWV_{REF_CAL}, Fig. 5(d)–(f) shows the comparisons of the original and calibrated MOD2 IR retrievals with PWV_{GPS} and PWV_{ERA} over both ocean and land, respectively. For the calibrations under wet atmosphere (i.e., MOD2), the overcalibration of PWV_{LS} is improved. Comparisons of PWV_{LS} against PWV_{GPS} show that the STD of the mean difference decreases from 7.48 to 5.69 mm, together with the RMS difference reduction from 12.52 to 5.58 mm (see Table II). In addition, comparisons of PWV_{LS} with PWV_{ERA} over both land and ocean also reveal similar results. Moreover, when the DLCM is applied, the resulting PWV_{DLCM} appears to be closer to PWV_{REF_COM} than PWV_{LS}. The STD of the mean difference further decreases to 3.29, 4.56, and 3.41 mm; and the RMS difference further reduces to 4.48, 8.98, and 4.75 mm, respectively. Thus, further improvements are achieved for MOD2 calibration after the DLCM was implemented.

As described above, PWV_{ERA} can be also selected as PWV_{REF_CAL}. Fig. 6(a) and (b) shows the comparisons of the original and calibrated MOD1 IR retrievals with PWV_{GPS} and PWV_{ERA}, respectively; and Fig. 6(c) and (d) shows the comparisons for MOD2. As shown in Fig. 6, both PWV_{LS} and PWV_{DLCM} can relieve the deviations of PWV_{ORIG} from PWV_{REF_COM} for MOD1 and MOD2 successfully. After implementation of the LS model, the STD of the mean difference decreases from originally 2.65 and 3.90 mm to 1.59 and 2.34 mm for MOD1 and from originally 7.48 and 10.23 mm to 6.09 and 8.33 mm for MOD2, and the RMS difference drops from originally 2.81 and 4.63 mm to 2.12 and 2.34 mm for MOD1 and from originally 12.52 and 16.10 mm to 6.01 and 8.36 mm for MOD2 (see Table II), respectively, when comparing PWV_{LS} with PWV_{GPS} and PWV_{ERA}. Furthermore, as shown in Fig. 6 and Table II, the performance of PWV_{DLCM} is again better than that of PWV_{LS} during both internal and external coincidence comparisons. Taking the external coincidence comparisons as example, the STD of the mean difference between PWV_{DLCM} and PWV_{GPS} further decreases to

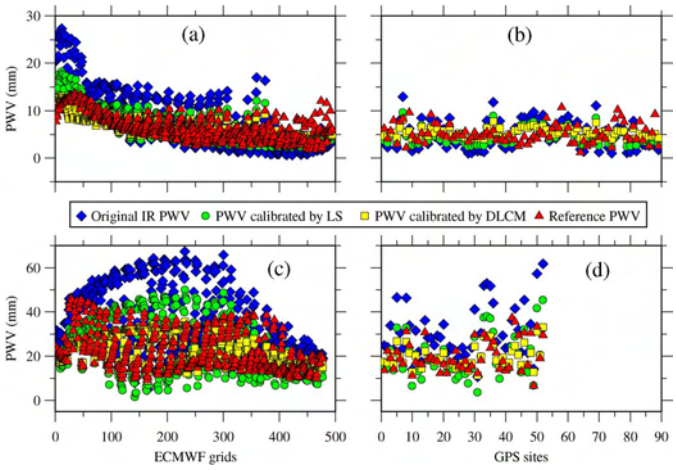

Fig. 6. Calibrations of MODIS IR PWV measurements in midlatitude regions when PWV_{ERA} is used as PWV_{REF_CAL}. The original and calibrated MOD1 PWV measurements were compared with (a) PWV_{ERA} and (b) PWV_{GPS}, respectively. (c) and (d) Similar to (a) and (b), but for MOD2.

0.92 mm [see Fig. 6(a)] and 3.18 mm [see Fig. 6(c)] for MOD1 and MOD2, and the corresponding RMS difference also reduces to 1.87 mm [see Fig. 6(a)] and 4.50 mm [see Fig. 6(c)], respectively. The encouraging results indicate that not only can the DLCM calibrate the IR retrievals effectively but it also avoids the overcalibrations of the LS model.

C. Case Studies at Low Latitude

When PWV_{GPS} is used as PWV_{REF_CAL}, comparisons of the original and calibrated IR retrievals with PWV_{GPS} and PWV_{ERA} over both ocean and land under dry atmosphere in equatorial region (i.e., MOD3) are shown in Fig. 7(a)–(c), and those comparisons under wet atmosphere in equatorial region (i.e., MOD4) are illustrated in Fig. 7(d)–(f). As shown in Fig. 7(a)–(c), both the LS model and the DLCM calibrate PWV_{ORIG} effectively. However, unlike the cases in midlatitude

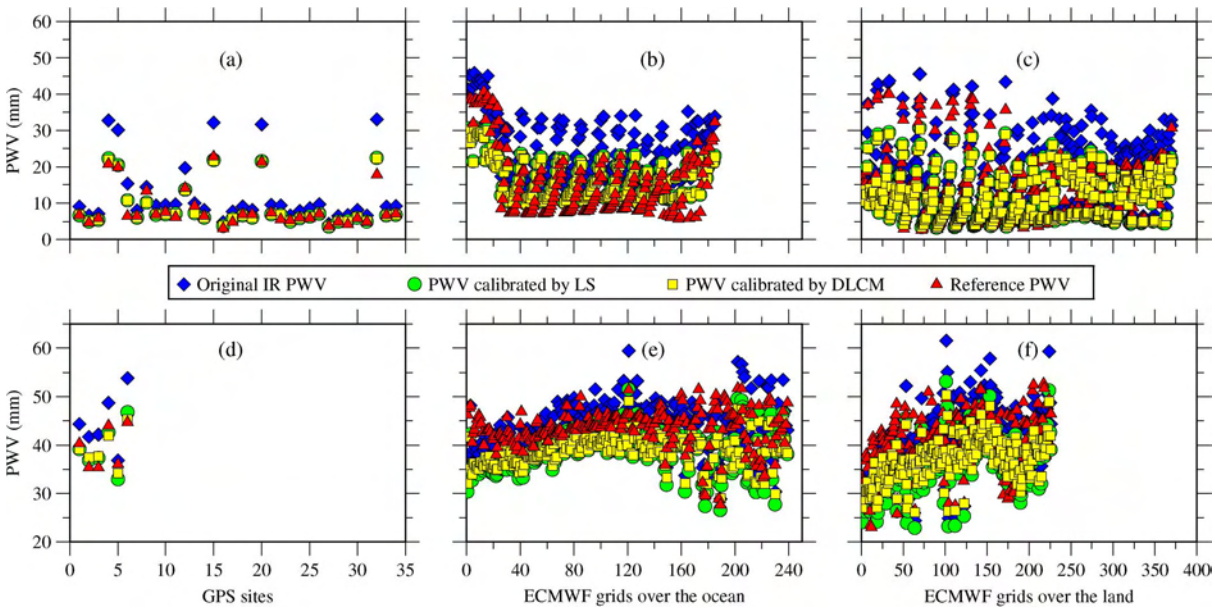

Fig. 7. Calibrations for MODIS IR PWV measurements at low latitude when PWV_{GPS} is used as PWV_{REF_CAL}. The original and calibrated MOD3 PWV measurements were compared with (a) PWV_{GPS} and PWV_{ERA} over both (b) ocean and (c) land, respectively. (d)–(f) Similar to (a)–(c), but for MODIS water vapor field under wet atmosphere (i.e., MOD4).

region, the performance of the DLCM has not shown overwhelming advantages over the LS model. Internal coincidence comparison [see Fig. 7(a)] between PWV_{DLCM} and PWV_{GPS} shows slightly better performance than the comparison between PWV_{LS} and PWV_{GPS} (see Table II), whereas external coincidence comparisons [see Fig. 7(b) and (c)] between PWV_{DLCM} and PWV_{ERA} over both ocean and land get worse than the comparisons between PWV_{LS} and PWV_{ERA} over both ocean and land (see Table II). Moreover, similar results have been also observed for MOD4 [see Fig. 7(d)–(f)], except that PWV_{LS} is again overcalibrated during the external coincidence comparisons with PWV_{ERA} over both ocean and land (i.e., the RMS differences increase from originally 5.02 to 6.09 mm and from originally 3.75 to 5.77 mm, respectively; see Table II). The possible reason for the inferior and unsuccessful calibrations of MOD3 [see Fig. 7(b) and (c)] and MOD4 [i.e., Fig. 7(e) and (f)] with the DLCM may be the low density and uneven distribution of selected PWV_{REF_CAL} (i.e., PWV_{GPS} in Fig. 7).

In another aspect, when the equally distributed PWV_{ERA} is used as PWV_{REF_CAL}, the performances of calibrated measurements for MOD3 and MOD4 are shown in Fig. 8 and Table II. It is clear from Fig. 8 that the choice of PWV_{ERA} as PWV_{REF_CAL} still cannot avoid the overcalibration of the LS model. Taking MOD4 as an example, during the comparisons of PWV_{LS} with PWV_{GPS} and PWV_{ERA}, the STD of the mean difference deteriorates by 24.4% and 24.5%, and the RMS difference worsens by 11% and 20.9%, respectively [see Fig. 8(c) and (d) and Table II]. However, unlike the limited improvements or bad performance of the LS model, the DLCM works robust for calibrating the IR retrievals of MOD3 and MOD4. Comparisons of PWV_{DLCM} with PWV_{GPS} and PWV_{ERA} show that STD improvements of 23.4% and 23.2% for MOD3 and 42% and 42.2% for MOD4 and RMS improvements of 63.2% and 38.1% for MOD3 and 22.4% and 15.9% for MOD4 have been achieved, respectively. The improvements of the DLCM calibrated PWV measurements again show that when the well-distributed reference PWV measurements (i.e., PWV_{ERA} in Fig. 8) are selected, the DLCM can calibrate the MODIS IR retrievals effectively.

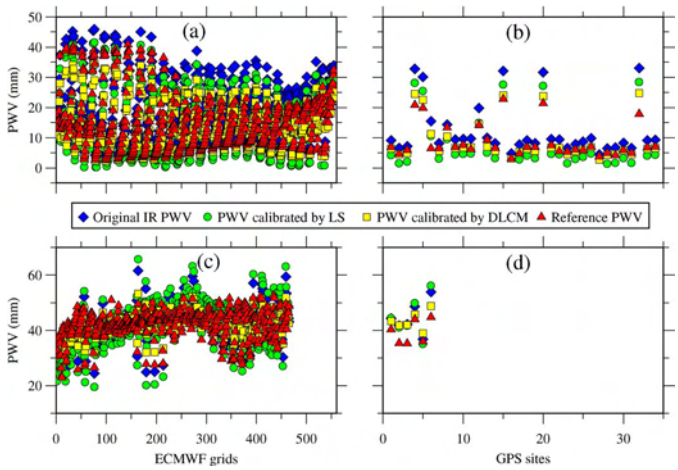

Fig. 8. Calibrations for MODIS IR PWV measurements at low latitude when PWV_{ERA} is used as PWV_{REF_CAL}. The original and calibrated MOD3 PWV measurements were compared with (a) PWV_{ERA} and (b) PWV_{GPS}, respectively. (c) and (d) Similar to (a) and (b) but for MOD4.

V. Conclusion

In this paper, we have developed the DLCM to calibrate the PWV measurements from MODIS IR water vapor product during the nighttime. We conduct analysis to correct the MODIS IR retrievals at nighttime on four scenes considering both dry and moist atmosphere in midlatitude and equatorial regions with the DLCM. Our findings from this study can be summarized as follows.

1) Comparisons of IR retrievals during the nighttime with ERA-Interim-, GPS-, and radiosonde-derived PWV

measurements show RMS of 3.28, 2.61, and 2.66 mm and STDs of 2.71, 1.92, and 2.30 mm, respectively. The large uncertainties of MODIS IR retrievals indicate that the MODIS IR water vapor product should be calibrated before being applied to monitor water vapor at night.

2) When PWV_{GPS} is used as PWV_{REF_CAL}, the performance of the LS model appears to be unstable since the corrected PWV values are overcalibrated from time to time (e.g., MOD1 and MOD4). Selecting PWV_{ERA} as PWV_{REF_CAL}, the LS model works well for MOD1 and MOD2, but it again leads to the overcalibrated PWV measurements for MOD3 and MOD4. As such, despite that the LS model has been proven to be an effective model for MODIS nIR water vapor product correction, it is confirmed in this paper that this model is not the prime choice for MODIS IR retrievals calibration.
3) In general, the proposed DLCM can avoid the overcalibration of MODIS IR PWV measurements effectively. However, when the sparse covered PWV_{GPS} is used as PWV_{REF_CAL} in equatorial regions, the performance of the DLCM calibrated IR retrievals is also unsatisfactory.
4) One of the crucial factors for the successful calibration of the proposed DLCM is the high density of PWV_{REF_CAL}. By selecting the global equally distributed PWV_{ERA} rather than PWV_{GPS} as PWV_{REF_CAL}, more accurate calibrated MODIS IR retrievals at nighttime can be expected.

However, calibrations of MODIS IR water vapor product with the DLCM over high-latitude regions were not demonstrated and analyzed in this paper. Although the ERA-Interim analysis data were globally distributed and can be used for building the DLCM and calibrating the IR retrievals, no proper data were found to objectively assess the calibration (e.g., only a few GPS stations were located near the Arctic and Antarctica regions). Furthermore, the low frequency of the MODIS cloud-free condition in both the Arctic and Antarctica regions [22], [23] may be another limitation to the application of the DLCM in high-latitude regions.

ACKNOWLEDGMENT

The authors would like to thank Prof. A. Plaza and the other two anonymous reviewers for their guiding and constructive comments.

REFERENCES

[1] M. T. Chahine, "The hydrological cycle and its influence on climate," *Nature*, vol. 359, pp. 373–380, Oct. 1992.
[2] O. Bock *et al.*, "Multiscale analysis of precipitable water vapor over Africa from GPS data and ECMWF analyses," *Geophys. Res. Lett.*, vol. 34, no. 9, pp. L09705-1–L09705-6, May 2007.
[3] J. Wang, L. Zhang, A. Dai, T. Van Hove, and J. Van Baelen, "A near-global, 2-hourly data set of atmospheric precipitable water from ground-based GPS measurements," *J. Geophys. Res.*, vol. 112, no. D11, p. D11107, Jun. 2007.
[4] J. Wang *et al.*, "Corrections of humidity measurement errors from the Vaisala RS80 radiosonde—Application to TOGA COARE data," *J. Atmos. Ocean. Technol.*, vol. 19, no. 7, pp. 981–1002, Jul. 2002.
[5] D. J. Gaffen, T. P. Barnett, and W. P. Elliott, "Space and time scales of global tropospheric moisture," *J. Clim.*, vol. 4, no. 10, pp. 989–1008, Oct. 1991.
[6] Z. Li, J. P. Muller, and P. Cross, "Comparison of precipitable water vapor derived from radiosonde, GPS, Moderate Resolution Imaging Spectroradiometer measurements," *J. Geophys. Res.*, vol. 108, no. D20, pp. 4651–4663, Oct. 2003.
[7] J. Duan *et al.*, "GPS meteorology: Direct estimation of the absolute value of precipitable water," *J. Appl. Meteorol.*, vol. 35, no. 6, pp. 830–838, Jun. 1996.
[8] R. H. Ware *et al.*, "Suominet: A real-time national GPS network for atmospheric research and education," *Bull. Amer. Meteorol. Soc.*, vol. 81, no. 4, pp. 677–694, Apr. 2000.
[9] Y. J. Kaufman and B. C. Gao, "Remote sensing of water vapor in the near IR from EOS/MODIS," *IEEE Trans. Geosci. Remote Sens.*, vol. 30, no. 5, pp. 871–884, Sep. 1992.
[10] R. Lindstrot *et al.*, "1D-Var retrieval of daytime total columnar water vapour from MERIS measurements," *Atmos. Meas. Tech.*, vol. 5, no. 3, pp. 631–646, Mar. 2012.
[11] S. Bedka, R. Knuteson, H. Revercomb, D. Tobin, and D. Turner, "An assessment of the absolute accuracy of the Atmospheric Infrared Sounder v5 precipitable water vapor product at tropical, midlatitude, arctic ground-truth sites: September 2002 through August 2008," *J. Geophys. Res.*, vol. 115, no. D17, pp. D17310-1–D17310-17, Sep. 2010.
[12] F. Aires, W. B. Rossow, N. A. Scott, and A. Chedin, "Remote sensing from the infrared atmospheric sounding interferometer instrument: 2. Simultaneous retrieval of temperature, water vapor, ozone atmospheric profiles," *J. Geophys. Res.*, vol. 107, no. D22, pp. ACH 7-1–ACH 7-12, Nov. 2002.
[13] A. Somieski *et al.*, "Tropospheric water vapor from solar spectrometry and comparison with Jason microwave radiometer measurements," *J. Geophys. Res.*, vol. 111, no. D9, pp. D09104-1–D09104-11, May 2006.
[14] G. W. Petty and K. Li, "Improved passive microwave retrievals of rain rate over land and ocean. Part I: Algorithm description," *J. Atmos. Ocean. Technol.*, vol. 30, no. 11, pp. 2493–2508, Nov. 2013.
[15] R. G. Kleidman *et al.*, "Remote sensing of total precipitable water vapor in the near-IR over ocean glint," *Geophys. Res. Lett.*, vol. 27, no. 17, pp. 2657–2660, Sep. 2000.
[16] N. Lu *et al.*, "On the use of GPS measurements for Moderate Resolution Imaging Spectrometer precipitable water vapor evaluation over southern Tibet," *J. Geophys. Res.*, vol. 116, no. D23, pp. D23117-1–D23117-7, Dec. 2011.
[17] S. W. Seemann, J. Li, W. P. Menzel, and L. E. Gumley, "Operational retrieval of atmospheric temperature, moisture, ozone from MODIS infrared radiances," *J. Appl. Meteorol.*, vol. 42, no. 8, pp. 1072–1091, Aug. 2003.
[18] S. H. Chen, Z. Zhao, J. S. Haase, A. D. Chen, and F. Vandenberghe, "A study of the characteristics and assimilation of retrieved MODIS total precipitable water data in severe weather simulations," *Mon. Weather Rev.*, vol. 136, no. 9, pp. 3608–3628, Sep. 2008.
[19] A. K. Prasad and R. P. Singh, "Validation of MODIS Terra, AIRS, NCEP/DOE AMIP-II Reanalysis-2, AERONET Sun photometer derived integrated precipitable water vapor using ground-based GPS receivers over India," *J. Geophys. Res.*, vol. 114, pp. D05107-1–D05107-20, Mar. 2009.
[20] D. P. Dee *et al.*, "The ERA-Interim reanalysis: Configuration and performance of the data assimilation system," *Q. J. R. Meteorol. Soc.*, vol. 137, no. 656, pp. 553–597, Apr. 2011.
[21] R. Z. Bar-Or, O. Altaratz, and I. Koren, "Global analysis of cloud field coverage and radiative properties, using morphological methods and MODIS observations," *Atmos. Chem. Phys.*, vol. 11, pp. 191–200, Jan. 2011.
[22] D. H. Bromwich *et al.*, "Tropospheric clouds in Antarctica," *Rev. Geophys.*, vol. 50, no. 1, pp. RG1004-1–RG1004-40, Mar. 2012.
[23] M. A. Chan and C. C. Josefino, "Arctic cloud characteristics as derived from MODIS, CALIPSO, CloudSat," *J. Clim.*, vol. 26, no. 10, pp. 3285–3306, May 2013.

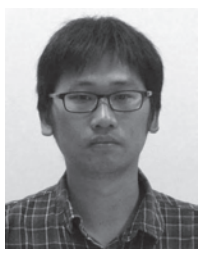

Liang Chang (M'14) was born in Hubei, China, in 1984. He received the B.Eng. degree in surveying and mapping engineering from the Nanjing University of Technology, Nanjing, China, in 2006 and the Ph.D. degree in geodesy and surveying engineering from Hohai University, Nanjing, in 2011.

From July 2011 to May 2013, he was a Postdoctoral Fellow with the Shanghai Astronomical Observatory, Chinese Academy of Sciences, Shanghai, China. He is currently a Lecturer with the College of Marine Sciences, Shanghai Ocean University, Shanghai. He is also currently with the Collaborative Innovation Center for Distant-water Fisheries, Shanghai. His research interests include synthetic aperture radar interferometry and satellite oceanography.

Guoping Gao was born in Jiangsu, China, in 1972. He received the B.Sc. degree in meteorology from the Ocean University of China, Qingdao, China, in 1994 and the Ph.D. degree in marine science from the University of Massachusetts, Dartmouth, MA, USA, in 2011.

From July 1994 to March 2005, he was an Engineer in ocean observation with the Ocean University of China. From March 2005 to September 2006, he was a Visiting Scholar with the University of Massachusetts. He is currently a Professor with the College of Marine Sciences, Shanghai Ocean University, Shanghai, China. He is also currently with the Collaborative Innovation Center for Distant-water Fisheries, Shanghai. His main research areas include ocean observation, ocean modeling, ocean dynamics, and ice–ocean interaction.

Shuanggen Jin was born in Anhui, China, in 1974. He received the B.Sc. degree in geodesy/geomatics from Wuhan University, Wuhan, China, in 1999 and the Ph.D. degree in global navigation satellite system/geodesy from the University of Chinese Academy of Sciences, Beijing, China, in 2003.

Since 2004, he has been a Visiting Fellow with the University of New South Wales, Sydney, Australia; a Postdoctoral and Senior Scientist with the Korea Astronomy and Space Science Institute, Daejeon, Korea; a Professor with the Korea University of Science and Technology, Daejeon; and a Research Fellow with the Center for Space Research, University of Texas at Austin, Austin, TX, USA. He is currently a Professor with the Shanghai Astronomical Observatory, Chinese Academy of Sciences, Shanghai, China, and the Director of the Center for Space Geodesy, China University of Mining and Technology, Xuzhou, China. His main research areas include satellite navigation, remote sensing, satellite gravimetry, and space/planetary sensing and soft/hardware development for wide applications.

Dr. Jin has been the President of the International Association of Planetary Sciences (2013–2015), the President of the International Association of Geodesy Sub-Commission 2.6 (2011–2015), the Editor-in-Chief of the *International Journal of Geoscience* (since 2010), the Associate Editor-in-Chief of *Satellite Navigation* (since 2013), an Associate Editor of *Advances in Space Research* (since 2013), and an Editorial Board Member of five other international journals.

Xiufeng He received the B.Eng. and M.S. degrees in control and navigation from the Nanjing University of Aeronautics and Astronautics, Nanjing, China, in 1986 and 1989, respectively, and the Ph.D. degree in navigation and survey engineering from Hong Kong Polytechnics University, Hong Kong, in 1998.

In the period of 1998–1999, she was a Postdoctoral Fellow with the Norwegian University of Science and Technology, Trondheim, Norway, where she was working in guidance, navigation, and control. In 2000, she was a Research Fellow with the Global Positioning System (GPS) Center, Nanyang Technological University, Singapore. She is currently a Professor and the Director of the Institute of Satellite Navigation and Spatial Information, Hohai University, Nanjing. She has authored or coauthored three books and over 130 referred papers. Her main research interests include interferometric synthetic aperture radar, global navigation satellite system (GNSS) [GPS and GLObal NAvigation Satellite System], inertial navigation system (INS), and the low-cost integrated GNSS/INS navigation system.

Ruya Xiao was born in Henan, China, in 1987. He received the B.Eng. degree in surveying and mapping engineering from Hohai University, Nanjing, China, in 2005. He is currently working toward the Ph.D. degree in the School of Earth Sciences and Engineering, Hohai University.

In the period from 2012 to 2013, he was a Research Assistant with the Institute of Space and Earth Information Science, The Chinese University of Hong Kong, Hong Kong. His research interests include deformation monitoring using synthetic aperture radar interferometry time-series analysis and Global Positioning System.

Lixin Guo, photograph and biography not available at the time of publication.